Subject catagory:
1. Simulations for Nano Systems (Non-optical)
2. Nano Material Fabrication and Applications

Experimental matching method for the two-dimensional numerical simulation of micro-floating zone in laser heated pedestal

P. Y. Chen[1], C. L. Chang [2], and S. L. Huang[24] ,C. W. Lan[3]
[1]Department of Gemology, Meiho University, Pingtung 91202, Taiwan
[2]Institute of Photonic & Optoelectronics, National Taiwan University, Taipei 10617, Taiwan
[3]Department of Chemical Engineering, National Taiwan University, Taipei 10617, Taiwan
[4]Department of Electrical Engineering, National Taiwan University, Taipei 10617, Taiwan
x00008415@meiho.edu.tw

ABSTRACT

It has been verified by comparing with the shape of the molten zone in terms of the experiment and then analyze the simulation results. That is experimental matching method.

The two-dimensional simulation was employed to study the melt/air and melt/solid interface shapes of the miniature molten zone formed in the laser-heated pedestal growth (LHPG) system. Using non-orthogonal body-fitting grid system with control-volume finite difference method, the interface shape can be determined both efficiently and accurately. During stable growth, the dependence of the molten-zone length and shape on the heating CO_2 laser is examined in detail under both the maximum and the minimum allowed powers with various growth speeds.

Finally, heat transfer and fluid flow in the LHPG system are analyzed near the deformed interfaces. The global thermal distributions of the crystal fiber, the melt, and the source rod are described by temperature and its axial gradient within length of ~10 mm. As compared with the growth of bulk crystal of several centimeters in dimension, natural convection drops six orders in magnitude due to smaller melt volume; therefore, conduction rather than convection determines the temperature distribution in the molten zone. Moreover, thermocapillary convection rather than mass-transfer convection becomes dominant. The symmetry and mass flow rate of double eddy pattern are significantly influenced by the molten-zone shape due to the diameter reduction and the large surface-tension-temperature coefficient in the order of 10^{-4}~10^{-3}. According to the analysis shown as above, the results could be further extended for the analysis of the concentration profile and study of horizontal growth.

Keywords: experimental matching method, interface shape, laser-heated pedestal growth, YAG, single-crystal fiber, heat transfer, fluid flow

1. INTRODUCTION

Single-crystal fibers have become the subject of intense study recently. They have been recognized to possess remarkable characteristics. Some applications for passive devices [1] and active devices [2-4] have been made in our group. Laser-heated pedestal growth (LHPG) method [5,6] are the crucible-free technique with the main advantages including high pulling rates, low production cost, and the feasibility of growing materials with very high melting points, high purity and low stress.

2. EXPERIMENTAL APPROACH

Figure 1 illustrates the LHPG method [7,9] for growing single-crystal fibers. An 100-W, 10.6-μm, linearly-polarized CO_2 laser system was the heat source to enter the growth chamber. A new source rod of smaller diameter can be obtained by a pre-growth process. The source rods were cut from yttrium aluminum garnet ($Y_3Al_5O_{12}$; YAG) crystals and the seed rods in <111> direction were utilized to dictate the crystallographic orientation.

3. MATHEMATICAL FORMULATION

Figure 2 (a) illustrates the LHPG's growth chamber. Figure 2 (b) illustrates the micro-floating zone in the LHPG system. The ambient temperature is constant. Thermal convection is symmetric axially, laminar at a pseudo-steady state. The oscillation of thermocapillary convection is neglected. Furthermore, gravity and 2D cylindrical coordinate are considered. Three governing equations are listed below [8,11]:

Equation of motion,

$$\frac{\partial}{\partial r}\left(\frac{\omega}{r}\frac{\partial\psi}{\partial z}\right)-\frac{\partial}{\partial z}\left(\frac{\omega}{r}\frac{\partial\psi}{\partial r}\right)+\frac{\partial}{\partial r}\left[\frac{1}{r}\frac{\partial}{\partial r}(\mu_m r\omega)\right]+\frac{\partial}{\partial z}\left[\frac{1}{r}\frac{\partial}{\partial r}(\mu_m r\omega)\right]-\rho_m\beta_m g\frac{\partial T}{\partial r}=0. \quad (1)$$

Stream function,

$$\frac{\partial}{\partial z}\left(\frac{1}{\rho_m r}\frac{\partial\psi}{\partial z}\right)+\frac{\partial}{\partial r}\left(\frac{1}{\rho_m r}\frac{\partial\psi}{\partial r}\right)+\omega=0. \quad (2)$$

Energy function,

$$\frac{\partial}{\partial r}\left(C_{pm}T\frac{\partial\psi}{\partial z}\right)-\frac{\partial}{\partial z}\left(C_{pm}T\frac{\partial\psi}{\partial r}\right)+\frac{\partial}{\partial z}\left(rk_{s,m}\frac{\partial T}{\partial z}\right)+\frac{\partial}{\partial r}\left(rk_{s,m}\frac{\partial T}{\partial r}\right)=0. \quad (3)$$

where ψ, ω, μ_m, ρ_m, β_m, C_{pm}, T, and $k_{s,m}$ are the stream function (g s^{-1}), vorticity, viscosity of melt, density of melt, thermal expansion coefficient of melt, specific heat of melt, temperature, and thermal conductivity of solid or melt, respectively. Moreover, the radial velocity, axial velocity, and vorticity are u, υ, and ω, respectively:

$$u=-\frac{1}{\rho_L r}\frac{\partial\psi}{\partial z},\upsilon=\frac{1}{\rho_L r}\frac{\partial\psi}{\partial r},\omega\equiv\frac{\partial u}{\partial z}-\frac{\partial\upsilon}{\partial r}. \quad (4)$$

Three thermal and fluid boundary conditions are (1) along z axis, (2) at the melt/solid interface, and (3) on the surfaces of the source rod, the melt, and the crystal fiber. There is additional thermal condition far away from the melt. The laser intensity profile on the miniature MZ is an asymmetrical Gaussian distribution,

$$I_a=A_q\exp\left[-\alpha_a(z/\gamma_a)^2\right]. \quad (5)$$

where A_q and γ_a are the amplitude and Gaussian width ($1/e^2$) at $z=0$, and α_a is the beam-shape factor.

4. RESULT AND DISCUSSION

4.1 Comparison between experiments and simulations

Figure 3 (1) shows a comparison between experiments and simulations on the molten-zone lengths at various laser powers for different reduction ratios. The source rod size is 300 μm and the feed speed is 1.2 mm per minute. The reduction ratios are 100%, 35%, and 25% for (a), (b), and (c), respectively. When normalized to the source-rod diameter, the allowed molten-zone lengths are 1.07-1.53 in (a), 1.07-1.72 in (b), and 0.67-1.46 in (c). By decreasing the reduction ratios, the allowed laser power is lower. We are also aware that the maximum length of the molten zone divided by the minimum length is 2±0.5 for stable growth. Similar empirical criteria have been introduced previously. The contact angle at the tri-point and the surface tension depend on the ability of the material to restrict variations in the melt/air interface shape. For fixed contact angle, the shapes of the melt/air interface and the molten-zone length can be varied by changing the laser power or reduction ratios. The upper melt/solid interface is more convex toward the melt can be obtained at lower growth speed and is determined by both the temperature gradient normal to the melt/solid interface and the release of the latent heat. Figure 3 (2) shows a comparison between experiments and simulations on the normalized radial and axial positions where the free surfaces are located at H_b in Figure 3 (1) (b). For clear comparison, the positions are normalized by the length of the molten zone axially and the maximum radius of the molten zone radially. The azimuthal area and shape of the free surface are in good agreement between the experiments and simulations. Figure 3 (3) shows a comparison of molten-zone length between experiments and simulations at various laser powers with semi- and asymmetric Gaussian distributions. The source rod size is 400×400 μm and the feed speed is 4 mm per minute. The reduction ratios is 64%. For all cases, it is assumed that vaporization is neglected. The stable growth means the conditions that the usable crystal fibres can be produced successfully. To have a stable growth, the molten zone length can vary depending on the laser power. The slope of the linear dependence is defined as η. Greater η means more energy stored in the melt under dynamic equilibrium to extend the molten-zone length and raise the average temperature.

Figure 4 (a) shows η at various reduction ratios for different feed speeds with the reduction ratio of 35%. If the feed and growth speeds are zero, the heat energy is stored in the melt, and this situation results in the largest value of η for a reduction ratio of less than 70%. With the same source rod and feed speed, the increase in η becomes saturated by decreasing the reduction ratio, because the cross section at the melt/solid interface becomes smaller. The parabolic trend of η indicates that is inversely proportional to the cross section of the upper melt/solid interface. By increasing the feed speed, η decreases at a reduction ratio of less than 70% but increases at a higher reduction ratio using the same source rod. The reason is that heat removal via mass-transfer convection is enhanced by increasing the feed speed at the lower reduction ratios. However, there is a trade-off between the mass transfer and the cross section at the melt/solid interface due to continuity. When increasing the feed speed, η becomes higher owing to the larger cross section at the melt/solid interface.

Figure 4 (b) shows the radial positions of the melt/air interface and the curvature radius at various axial positions with the reduction ratio of 35%. An inflection point can be identified by the peak value of the curvature radius at various axial positions. The melt/air interface is wine-bottle shaped. The higher peak value of the curvature radius means a smoother profile at the inflection point. Moreover, the axial position of the inflection point reveals the degree to which the molten zone extends radially at the bottom. The inflection point moves from ‘z < 0’ to ‘z > 0’ and the peak value of the curvature radius decreases as the laser power rises. The laser heating efficiency for the same melt volume can be improved if the laser beam is projected onto the position (z=0) near the location of the peak curvature radius.

Figure 4 (c) simulates the effect of gravity on the melt/air interface with the reduction ratio of 35%. There is almost no difference between normal and near-zero gravity. At H_b, surface tension shows an observable reduction in molten-zone length with near-zero gravity. The variation in the length of the molten zone due to gravity is much smaller than that effected by varying the laser power. Therefore, a variation in gravity along the growth direction will not obviously affect the stable conditions for growing crystal fibers.

4.2 Analysis of heat flow in the molten zone

Figure 5 shows T and dT/dz near the micro-floating zone at various axial positions for different reduction ratios when operating at high (H) and low (L) allowed laser power in the figure 3 (1). Where H_a, H_b, and H_c are 6.7 W, 2.2 W, 1.68 W, and 1.5 W. L_a, L_b, and L_c are 5.5 W, 2.05 W, 1.55 W, and 1.3 W. They represent the range of input laser powers for stable growth of crystal fibers.

The d*T*/d*z* reaches the maximum before the melt/solid interfaces because there is space for thermal flux to make a turn from radial to axial direction. As the reduction ratio decreases, the d*T*/d*z* distribution along z axis is closer to that along the melt/air interface. The growth/feed fronts can also be precisely identified by observing the local extremes of d*T*/d*z* due to the release/absorption of the latent heat. The differences in area under the curves of temperature distribution are smaller as the reduction ratio decreases because more internal energies stay near the z axis in the melt. The upper diagrams are corresponding streamlines and isotherms of the micro-floating zone. The patterns of the double eddy flow are almost symmetric when the reduction ratio is 100%. The temperature distribution is not influenced by fluid flow significantly because conduction is dominant rather than convection and radiation due to the small melt volume.

In static micro-floating zone ($U_{s,c} = 0$) without TC convection, only natural convection is formed with single eddy. The strongest mass flow rate is in the order of 10^{-9} g/s in the loop center and the peak temperature is about 2378 K. Figure 6 (a) shows the streamlines and isotherms for different $\partial\gamma/\partial T$ with the reduction ratio of 35%. The natural convection cannot be observed because its mass flow rate drops six orders in magnitude due to the miniature volume of micro-floating zone. The TC convection becomes stronger as $\partial\gamma/\partial T$ is increased. The stable double eddies are formed when the mass flow rate reaches the order of 10^{-6}~10^{-5} g s^{-1}. For YAG, $\partial\gamma/\partial T$ is -3.5×10^{-2} dyn cm^{-1} K^{-1} [12] and the resulting magnitude of mass flow rate are in the order of 10^{-5}~10^{-4} g s^{-1}, which is comparable to that in floating zone bulk crystal growth. The TC convection are in similar order because there is higher heat density using laser heating method, but smaller total melt/air interface area. Although the growth speed is much slower during the bulk crystal growth, the mass flow rate is still larger than that during the LHPG SCFs growth. In term of the induced mass flow rate among the three convections, TC ≥ mass-transfer >> natural is the typical behavior during the LHPG SCFs growth. Typically the lower eddy is formed faster than the upper one.

Figure 6 (b) shows the shapes of the melt/air interface with the reduction ratio of 35% by considering different kinds of thermal convections. At H_b, the discrepancy between curves 1~3 can clearly be observed. This is mainly due to the larger MZ volume and melt/air interface area for stronger mass-transfer and TC convections. At L_b, there is almost no difference between curves 4 and 5. For curve 6, the melt/air interface slightly becomes more convex outward due to the enhancement of the TC convection near the melt/air interface.

5. CONCLUSION

A two-dimensional simulation on the micro-floating zone fabricated using the LHPG method for growing single-crystal fibers was successfully verification from experimental matching method. The stable conditions utilized for producing a useful crystal fiber are defined. The effects caused by thermocapillary and mass-transfer convection in the melt and the trade-off between mass transfer and cross section at the melt/solid interface for heat dissipation are discussed. The melt/air interface is estimated and optimized for efficient laser absorption according to curvature radius and the inflection point. There is no significant change if the gravity is varied along the growth direction. The influence of gravity is discussed with reference to the feasibility of growing a crystal fiber horizontally.

Finally, heat transfer and fluid flow in the LHPG system are analyzed. Due to the small melt volume in the LHPG system, natural convection drops six orders in magnitude from several centimeters to hundred microns in dimension; therefore conduction rather than convection dominates the temperature distribution. TC convection rather than mass-transfer convection becomes dominant for large mass flow rate in the melt. Based on this work, the dopant concentration profile of the grown crystal fiber for active devices can be investigated further.

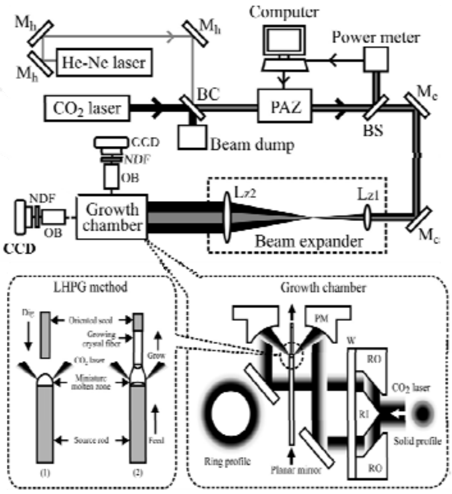

Fig. 1 The experimental layout of the LHPG system for growing single-crystal fibers.

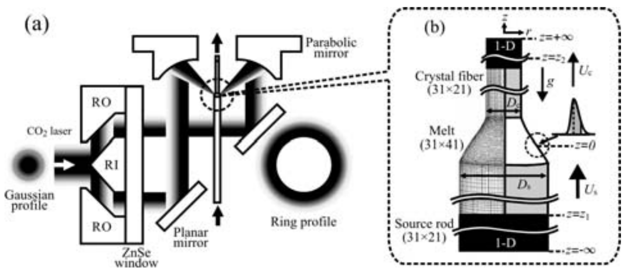

Fig. 2 (a) The illustration of the LHPG's growth chamber. RO and RI are the outer-cone and inner-cone reflaxicon; (b) The micro-floating zone in the curvilinear coordinate for the physical domain (left) and the sketch (right).

Subject catagory:
1. Simulations for Nano Systems (Non-optical)
2. Nano Material Fabrication and Applications

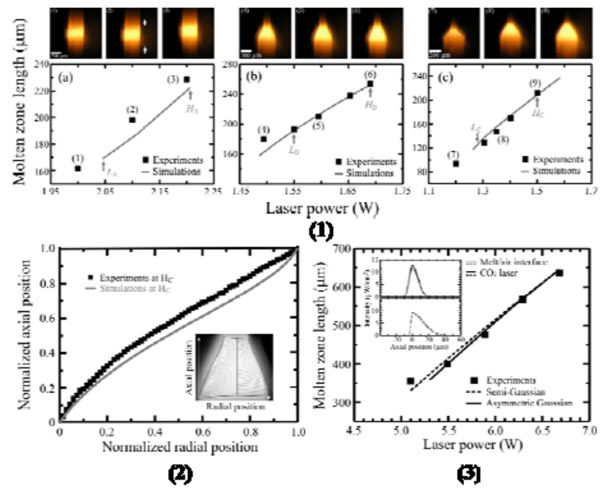

Fig. 3 (1) Micro-floating zone lengths at various laser powers for different reduction ratios in both experiments and simulations. The gray arrows labeled *H* and *L* are the higher and lower allowed laser powers. The upper indexed the captured images of the micro-floating zones correspond to those in Fig. (1). Fig. (2) The normalized radial and axial positions of the melt/solid interface in Fig. (1) at H_b in both experiments and simulations. The square dots in black represent the experimental results and the solid line in gray denotes the simulation result. The inset shows the image observed in the experiments overlapped by the isothermal lines at right side and the streamlines at left side in the simulations. Fig. (3) Micro-floating zone lengths at various laser powers with semi and asymmetric Gaussian distributions in both experiments and simulations. The solid and dashed lines indicate the profile in an asymmetric and semi-Gaussian distribution. The square dots represent the experimental data. The inset shows the two laser intensity profiles. The black lines denote the laser intensity profile and the gray lines denote the intensity profile on the free surface.

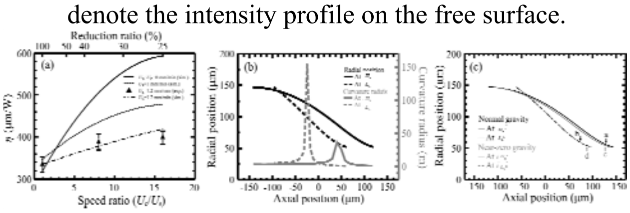

Fig. 4 (a) The slopes η at various reduction ratios for different feed speeds. (b) The radial positions and the curvature radius of the melt/air interface at various axial positions. (c) The radial positions of the melt/air interface at various axial positions.

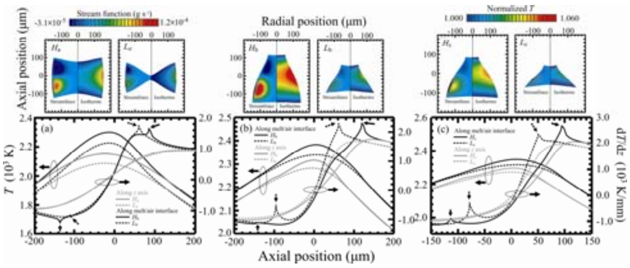

Fig. 5 *T* and d*T*/d*z* near the micro-floating zones at various axial positions for different reduction ratios when operating at *H* and *L* power. The upper diagrams are corresponding streamlines and isotherms of the micro-floating zones.

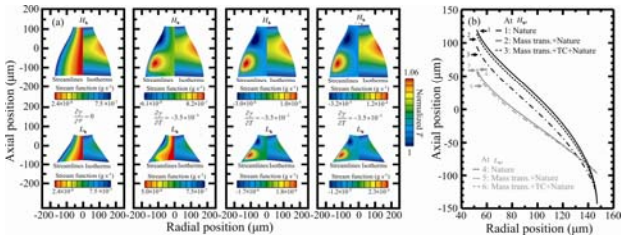

Fig. 6 (a) the streamlines and isotherms for different $\partial\gamma/\partial T$, and (b) the radial positions of the melt/air interface at various axial positions by involving different kinds of thermal convections with the reduction ratio of 35%.

6. ACKNOWLEDGMENTS

The authors gratefully acknowledge the support for this work in part by the National Science Council, Republic of China under contract number NSC 96-2628-E-002-042-MY3.

7. REFERENCES

[1] C. N. Tsai, Y. S. Lin, K. Y. Huang , Y. S. Lin, C. C. Lai, and S. L. Huang, **"**Enhancement of Cr^{4+} Concentration in $Y_3Al_5O_{12}$ Crystal Fiber by Pregrowth Perimeter Deposition,**"** *Jpn. J. Appl. Phys.*, vol. 47, pp. 6369-6373, 2008.

[2] C. C. Lai, K. Y. Huang, H. J. Tsai, K. Y. Hsu, S. K. Liu, C. T. Cheng, K. D. Ji, C. P. Ke, S. R. Lin, and S. L. Huang, **"**Yb^{3+}:YAG-silica fiber laser,**"** *Opt. Lett.*, vol. 34, pp. 2357-2359, 2009.

[3] K. Y. Huang, K. Y. Hsu, and S. L. Huang, **"**Analysis of ultra-broadband amplified spontaneous emissions generated by Cr^{4+}:YAG single and glass-clad crystal fibers,**"** *IEEE Lightwave Technol.*, vol. 26, pp. 1632-1639, 2008.

[4] L. M. Lee, S. C. Pei, D. F. Lin, M. C. Tsai, T. M. Tai, P. C. Chiu, D. H. Sun, A. H. Kung, and S. L. Huang, **"**Generation of tunable blue/green laser using ZnO:PPLN crystal fiber by self-cascaded second order nonlinearity,**"** *J. Opt. Soc. Am. B*, vol. 24, pp. 1909-1915, 2007.

[5] M. M. Fejer, J. L. Nightingale, G. A. Magel, and R. L. Byer, "Laser-heated miniature pedestal growth

apparatus for single-crystal optical fibers," *Rev. Sci. Instrum.* vol. 55, pp. 1791-1796, 1984.

[6] R. S. Feigelson, "Pulling optical fibers," *J. Cryst. Growth*, vol. 79, pp. 669-680, 1986.

[7] K. Y. Huang, K. Y. Hsu, D. Y. Jheng, W. J. Zhuo, P. Y. Chen, P. S. Yeh, and S. L. Huang, "Low-loss propagation in Cr^{4+}:YAG double-clad crystal fiber fabricated by sapphire tube assisted CDLHPG technique," *Opt. Express*, vol.16, pp. 12264-12271, 2008.

[8] P. Y. Chen, C. L. Chang, K. Y. Huang, C. W. Lan, W. H. Cheng, and S. L. Huang, "Experiment and simulation on interface shapes of an yttrium aluminium garnet miniature molten zone formed using the laser-heated pedestal growth method for single-crystal fibers," *J. Appl. Cryst.*, vol. 42, pp. 553-563, 2009.

[9] P. Y. Chen, C. L. Chang, C. W. Lan, W. H. Cheng, and S. L. Huang, "Two-Dimensional Simulations on Heat Transfer and Fluid Flow for Yttrium Aluminium Garnet Single-Crystal Fiber in Laser-Heated Pedestal Growth System," *Jpn. J. Appl. Phys.*, vol. 48, pp.115504, 2009.

[10] C. W. Lan and S. Kou, "Heat transfer, fluid flow and interface shapes in floating-zone crystal growth," *J. Cryst. Growth*, vol.108, pp.351-366, 1991.

[11] C. W Lan and S. Kou, "Thermocapillary Flow and Natural convection in a Melt Column with an Unkown Melt/Solid Interface," *Intern. J. Numer. Methods Fluids*, vol. 12, pp. 59-80, 1991.

[12] V. J. Fratello and C. D. Brandle, "Physical properties of a $Y_3A1_5O_{12}$ melt," *J. Cryst. Growth*, vol. 128, pp. 1006-1010, 1993.

國立中山大學
三十而立‧砥柱中流

2010 第十四屆 奈米工程暨微系統技術研討會論文集

The 14th Nano & Micro-System Technology Conference

網　址

http://www2.nsysu.edu.tw/nano2010

時　間

中華民國九十九年九月二日、九月三日

地　點

國立中山大學 圖書與資訊大樓11F

主辦單位

國立中山大學、工業技術研究院、中華民國微系統暨奈米科技協會

協辦單位

經濟部技術處、國家科學委員會、國立中山大學 機械與機電工程學系、
國立中山大學 工程技術研究推廣中心、國立中山大學 中山高醫跨校合作中心、
國立成功大學微奈米科技研究中心、國立屏東科技大學 材料工程學系、
國家實驗研究院 國家晶片系統設計中心、國家實驗研究院 國家奈米元件實驗室、
國家實驗研究院 儀器科技研究中心、國家實驗研究院 國家高速網路與計算中心、
國際半導體設備材料產業協會、中國鋼鐵股份有限公司、中華民國南部科學園區產學協會、
同欣電子工業股份有限公司

ITRI Industrial Technology Research Institute

NMA

目錄

序言

「第十四屆奈米工程暨微系統技術研討會」於 99 年 9 月 2-3 日假國立中山大學圖書資訊大樓舉辦。今年適逢中山大學 30 周年校慶,「三十而立 立如山石」在此而立之年承辦本屆研討會深具意義，謹在此對各界的支持致上最高的謝意。

第十四屆研討會規劃有四大會議主軸，分別是 A.奈米科技 B.生醫微流體 C.感測器與致動器及 D.微系統技術。承蒙各位教授先進及各級委員之協助，本屆研討會無論在投稿論文數及參與人數均有顯著成長，其中論文接受數為 196 篇，包含 96 篇口頭報告及 100 篇壁報論文。論文委員會並從投稿論文中推選 20 篇最佳論文獎入選論文，安排於各口頭報告場次中，並於入選論文中推薦 4 篇會議最佳論文及 8 篇佳作以茲鼓勵。大會並同步舉辦展覽會，以提供與會者最新之微奈米產品及設備訊息，所規劃之 22 個展覽攤位也由深耕國內之廠商全數承租，顯示國內微奈米研究之蓬勃發展與商業活力。

本屆會議特別邀請日本 Nagoya University 之 Kazuo Sato 教授、加拿大 Waterloo University 之 Dong-Qing Li 教授、現任職於香港 SAE Magnetics (HK) Ltd. 之黃瑞星教授以及大連理工大學的趙紀軍教授等分別擔任大會之 Keynote Speakers。此外，大會於會議結束後特別安排搭乘遊輪遊覽高雄港之活動，除提供一輕鬆、感性之時段讓與會者可以更進一步進行學術交流外，並讓與會者從海上遠眺中山大學依山傍海的校園與領略海洋首都高雄之美。

國立中山大學、工業技術研究院及中華民國微系統暨奈米科技協會誠摯感謝所有與會者，以及參與本屆會議之籌畫人員、協辦單位、贊助單位及參展廠商，因為有各方的協助使得大會得以順利進行。最後，敬祝所有與會者都能有豐碩的收穫與合作，並祝大家身體健康、工作順利。

國立中山大學機械與機電工程系 教授兼副研發長

林哲信

謹誌

主辦及協辦單位

主辦單位

國立中山大學

工業技術研究院

中華民國微系統暨奈米科技協會

協辦單位

經濟部技術處

國家科學委員會

國立中山大學 機械與機電工程學系

國立中山大學 工程技術研究推展中心

國立中山大學 中山高醫跨校研究中心

國立成功大學 微奈米科技研究中心

國立屏東科技大學 材料工程學系

國家實驗研究院 國家晶片系統設計中心

國家實驗研究院 國家奈米元件實驗室

國家實驗研究院 儀器科技研究中心

國家實驗研究院 國家高速網路與計算中心

國際半導體設備材料產業協會

中國鋼鐵股份有限公司

同欣電子工業股份有限公司

中華民國南部科學園區產學協會

籌備委員

主任委員:

楊弘敦

副主任委員:

光灼華、李世光、陳英忠、蔡新源

委員:

國家實驗研究院

江國寧、楊富量、蔡定平、魏慶隆

工研院

何宗哲、董靜宇、蘇宗粲

業界

余國寵、呂紹萍、孟憲鈺、林弘毅、
馬堅勇、陳玉松、陳立哲、蔡裕賢、蔡晴夫

學界：

方維倫、何扭今、李國賓
邱俊誠、張培仁、曾繁根

總幹事:

林哲信

副總幹事:

朱訓鵬、黃義佑

秘書組:

彭昭暐

論文委員

主任委員：

林哲信

委員：

朱俊勳、朱訓鵬、李　泉、林明澤
林哲信、邱　一、施文彬、范士岡
張凌昇、莊承鑫、傅龍明、游萃蓉
馮國華、黃義佑、楊燿州、鄒慶福
劉承賢、潘正堂、蘇宗粲、鍾震桂

資深委員：

方維倫、邱俊誠、李國賓、曾繁根

第 14 屆奈米工程暨微系統技術研討會大會議程

2010/9/2 Thursday	2010/9/3 Friday
報到 (0800~0830)	**Keynote 3** (Speaker: Ruey-Shing Huang) (0830~0930)
開幕 (0830~0900)	
Keynote 1 (Speaker: Kazuo Sato) (0900~1000)	Oral Session 3 (A~D 組) (0930~1100)
Break (1000~1030)	
Oral Session 1 (A~D 組) (1030~1200)	Break (1100~1120)
	Keynote 4 (Speaker:Ji-Jun Zhao) (1120~1220)
午餐(Lunch) (1200~1330)	午餐(Lunch) (1220~1330)
中華民國微系統暨奈米科技協會 會員大會 & Poster Session (1330~1430)	Oral Session 4 (A~D 組) (1330~1500)
Keynote 2 (Speaker: Dong-Qing Li) (1430~1530)	Poster Session (1500~1600)
Break (1530~1600)	
Oral Session 2 (A~D 組) (1600~1730)	高雄港乘船遊港 (Ferry Cruise) (1630~1830)
晚宴(Dinner) (1800~2000)	

校區平面圖

國立中山大學
三十而立·砥柱中流

會場平面配置圖

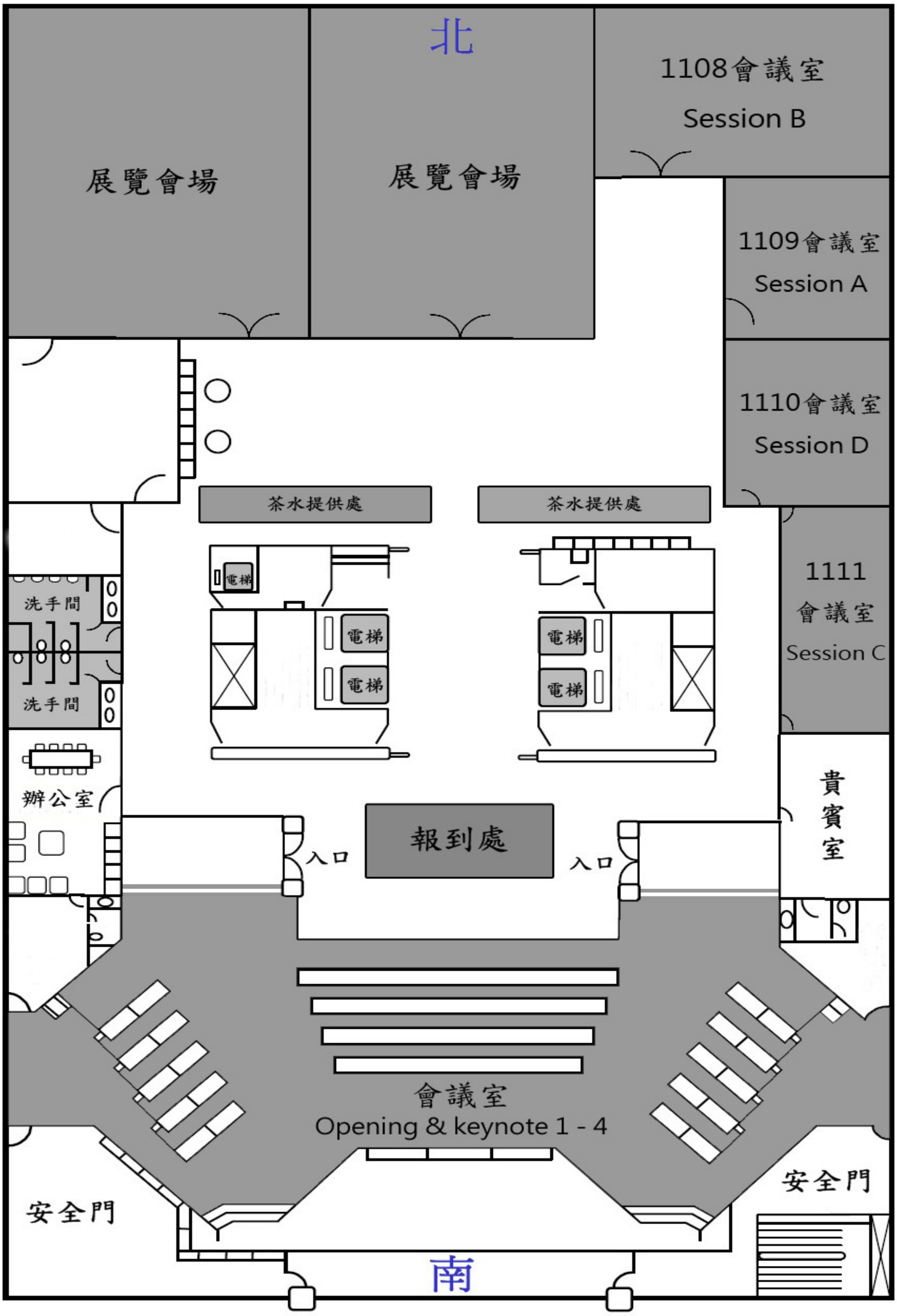
北
展覽會場
展覽會場
1108會議室
Session B
1109會議室
Session A
1110會議室
Session D
茶水提供處
茶水提供處
電梯
電梯
電梯
電梯
電梯
洗手間
洗手間
1111
會議室
Session C
辦公室
報到處
入口
入口
貴賓室
會議室
Opening & keynote 1 - 4
安全門
安全門
南

參展廠商攤位平面配置及編號

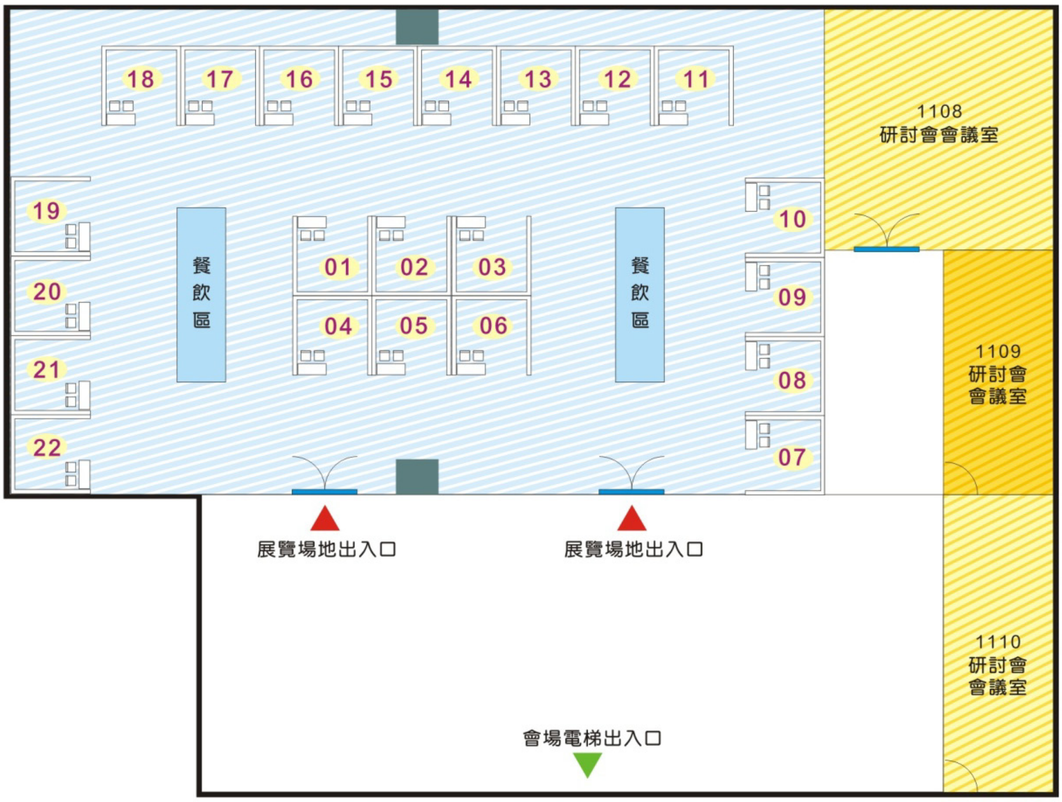

參展廠商攤位

- 01 王鼎精密股份有限公司
- 02 奕葉國際有限公司
- 03 昊青股份有限公司
- 04 汎達科技有限公司
- 05 景興電腦科技有限公司
- 06 國立虎尾科技大學
- 07 俊尚科技股份有限公司
- 08 德芮克國際股份有限公司
- 09 岱美亞洲公司
- 10 妙點企業股份有限公司
- 11 宇燦股份有限公司
- 12 國科企業有限公司
- 13 新皋企業股份有限公司
- 14 愛發股份有限公司
- 15 海金龍企業有限公司
- 16 元利儀器股份有限公司高雄分公司
- 17 技邦企業股份有限公司
- 18 富鑫奈米科技股份有限公司
- 19 三朋儀器股份有限公司
- 20 拉奇企業有限公司
- 21 磐拓國際股份有限公司
- 22 鑫陶應用材料有限公司

攤位編號	攤位名稱	展品名稱或公司主要業務	網址
1	王鼎精密股份有限公司	世界時區鐘錶機芯，精密微小塑膠射出零件，精密微小線圈，步進馬達，精密微電子組裝	www.atop9999.com.tw
2	奕葉國際有限公司	量測機台	www.probestaion.com
3	昊青股份有限公司	Mathematica, Origin, XFDTD	www.sciformosa.com.tw
4	汎達科技有限公司	可變焦觀察鏡頭	http://www.pentad.com.tw
5	景興電腦科技有限公司	日本 NEC 紅外線熱影像測溫儀 FS 系列. 高畫質影像顯微鏡 SS.高畫質影像工業內視鏡	http://www.chct.com.tw
6	國立虎尾科技大學	微系統暨奈米科技相關之研究成果	http://www.nfu.edu.tw
7	俊尚科技股份有限公司	原子層鍍膜設備、奈米鑽石鍍膜設備	http://www.junsun.com.tw
8	德芮克國際股份有限公司	粒徑及分散分析設備	www.trekintal.com.tw
9	岱美亞洲公司	代理國外儀器設備：產品包括 **1.**奈米碳管、奈米線、Graphene 成長設備、Thermal CVD、RTP **2.** 多功能材料測試儀 **3.**薄膜厚度測量儀 **4.**磁性測量儀 **5.**奈米級位移計 **6.**奈米級定位工作台 **7.**接觸 3D 表面輪廓測量儀 **8.**奈米級光學 3D 輪廓測量儀 **9.**光學式薄膜應力測量儀 10.防震台	www.dymek.com
10	妙點企業股份有限公司	代理振動相關領域測試設備。產品包含:振動測試機/振動控制品/微振加速規/光學位移感測器/運輸記錄器	http://www.magicdot.com.tw
11	宇燦股份有限公司	微機電分子氣相沉積系統(MVD)	http://www.ultrapro.com.tw/index.php

國立中山大學
三十而立·砥柱中流

12	國科企業有限公司	Kammrath & Weiss 顯微觀測材料試驗機、Agilent nano 奈米壓痕試驗機/奈米級萬能試驗機、MTS 微小力學試驗機	http://www.sinodynamics.com.tw/
13	新皋企業股份有限公司	原子力顯微鏡用探針	http://www.amplegoal.com.tw/
14	愛發股份有限公司	振動機、材料試驗設備、CAD/CAM/CAE 軟體	www.apic.com.tw
15	海金龍企業有限公司	SU8 photoresist ,OPV & OLED masterials , Aerosol Jet ,HF VPE,Novacentrix	www.gsdtec.com.tw
16	元利儀器股份有限公司高雄分公司	OLYMPUS OLS4000 雷射共軛焦點顯微鏡	http://www.yuanyu.com.tw/yuanli/Company.asp
17	技邦企業股份有限公司	各式 CCD、原子顯微鏡探針、光譜相機	www.keybond.com
18	富鑫奈米科技股份有限公司	1. 新世代奈米研磨分散設備及應用 2. 奈米分散液專業代工服務	www.justnano.com.tw
19	三朋儀器股份有限公司	1. 金相設備 2. 精密量測設備 3. 環境檢驗設備 4. 材料測試設備 5. 半導體檢測設備 6. 奈米相關設備 7. 原子力顯微鏡(AFM)8. 高速攝影機	www.sanpany.com.tw
20	拉奇企業有限公司	有機膜之聚對二甲苯氣相沉積系統設備(PARYLENE COATING MACHINE)	www.corecn.com.tw
21	磐拓國際股份有限公司	粉/液體, 軟質材料的特性分析儀器, 如粒徑分析儀、分散穩定性分析儀、微流變分析儀..等	www.titanex.com.tw
22	鑫陶應用材料有限公司	各種尖端材料, 如奈米材料, 導熱材料, 導電及金屬材料, 陶瓷材料..等	www.titanex.com.tw

第 14 屆奈米工程暨微系統技術研討會

分組研討議程表

一、口頭報告論文：

※敬請各位發表人，於各場會議開始前 15 分鐘將報告檔案放置會場電腦中。每篇論文報告時間為 12 分鐘，提問 3 分鐘，共 15 分鐘。

※有★標記為本屆論文獎候選名單

領域與場地	論文類別
A 奈米工程 (Room 1109)	01. Nano-electro-mechanical Devices and Systems
	02. Simulations for Nano Systems
	03. Nano Material Fabrication and Applications
B 生醫微流體 (Room 1108)	04. Fluidic Micro-components and Systems
	05. Micro Bio/Chemical Analysis Systems
	06. Microdevices for Power Supply and Energy Harvesting
C 微致動與傳感器 (Room 1111)	07. Mechanical, Thermal, Magnetic Sensors and Actuators
	08. Micro-optical Devices and Systems
	09. Wireless Communications Devices and Systems
D 微系統設計、製造封裝與材料技術 (Room 1110)	10. Design, Simulation and Testing
	11. Fabrication and Packaging Technologies
	12. Miscellaneous

Oral Session 1　9 月 2 日　10：00～10：30

A1 微系統技術	Nano Material Fabrication and Applications			
主持人: 朱訓鵬　游萃蓉		地點: Room 1109		
Time	**Paper ID**	**Title**	**Authors**	**Page**
10:30~10:45	A03_01	Diamond-like Nanocoposite (DLN) thin films for possible applications in MEMS/NEMS devices	T-S Santra, T-K Barik, F-G Tseng	41
10:45~11:00	A03_02	以氧化鋁為緩衝層增進填鐵奈米碳管叢之成長與填鐵效率	江衍諭、蘇志中、古昇灝、張所鋐	42
11:00~11:15	A03_03	★ 利用溶劑鑄造法製作出可控制性介孔隙材料	何宗承、張家榮、王本誠、曾繁根	43
11:15~11:30	A03_04	奈米孔洞應用於神經細胞之仿生結構晶片的研究	何符漢、盧彥蓓、林明瑜、歐育誠、楊中堯、葉哲良	44
11:30~11:45	A02_02	以密度泛涵理論研究具有 Stone-Wales 缺陷之（4，4）單壁碳化矽奈米管的機械和電子性質	朱訓鵬、王耀群、李家紘、邱敏甄	45
11:45~12:00	A03_06	★ Uniform Monolayer Deposition of Evaporable Droplet in Microwells for Fabricating Two-Dimensional Gold Nanoparticles Arrays	Y-Y Lin, C-Yi Lin, D-J Yao, F-G Tseng	46

B1 生醫微流體	Micro Bio/Chemical Analysis Systems			
主持人: 饒達仁　洪敏勝		地點: Room 1108		
Time	**Paper ID**	**Title**	**Authors**	**Page**
10:30~10:45	B05_01	Assessment on the Distance-Dependent Fluorescence Variation of DNA-Cy3-Tailored Gold Nanoparticles Deposited on a Solid Surface	J-M. Obliosca, P-C Wang, F-G Tseng	47
10:45~11:00	B05_08	★ A Novel Microchip System Integrated with Gold Nano-Electrode Ensemble for Electrochemical Determination of Hyaluronic Acid	Y-T Chuang, C-M Chen , C-S Chien, C-H Lin	48
11:00~11:15	B05_10	以介電泳微流體元件量測內皮細胞在膠原蛋白表面之貼附力	陳志彬、羅崇綱、洪敏勝	49
11:15~11:30	B05_11	Generation of Temporal Logarithmic Concentration for Dose-Response Assays on Electrophysiological Studies	C-Y Chen, T-Y Tu, D-S Jong, A-M. Wo	50
11:30~11:45	B05_12	奈米結構增強免標定式干涉式光纖生物感測器之靈敏度	陳聖杰、曾元泰、張勁淳、吳秉純、曾繁根	51
11:45~12:00	B05_14	★ Observation of Nanoparticles Dynamics in MicroWet-Cell Contained Solution under High Vacuum inside Electron Microscope and X-ray Microscope	T-W Huang, C-H Chu, G-C Yin, F-R Chen and F-G Tseng	52

C1 微致動與傳感器 Mechanical, Thermal, Magnetic Sensors and Actuators				
主持人: 李永春 楊燿州			地點: Room 1111	
Time	**Paper ID**	**Title**	**Authors**	**Page**
10:30~10:45	C07_14	★ 矽質撓性觸覺感測陣列之設計與實現	胡志帆、黃信瑀 溫志杰、林立元 方維倫	53
10:45~11:00	C07_09	Microfluidic Whole-cell Biosensor for Rapid Detection of Low-level Water Toxicity	T-C Chou, L-J Chien, C-H Chiou, J-T Tseng	54
11:00~11:15	C07_11	利用改良式溶膠凝膠塗佈法製作鋯鈦酸鉛壓電陶瓷厚膜	李永春、林峻毅	55
11:15~11:30	C07_13	Development of a 3D Distributed Carbon Nanotubes on Flexible Polymer for Normal and Shear Forces Measurement	W-S Su, C-F Hu, C-M Lin, and W-L Fang	56
11:30~11:45	C07_07	預防土石流預警系統之土壤含水量感測器之設計與製作	杜畯瑋、楊志安 黃建仁、馬榮華 李佳言	57
11:45~12:00	C07_17	★ 利用玻璃回融製程實現單軸全差分加速計	許義昌、孫志銘 林炯彣、徐家保 李侑道、蔡明翰 劉育嘉、方維倫	58

D1 微系統設計、製造封裝與材料技術 Design, Simulation and Testing				
主持人: 蘇育全 楊政達			地點: Room 1110	
Time	**Paper ID**	**Title**	**Authors**	**Page**
10:30~10:45	D10_05	毛細力驅動於矩形直流道的解析與實驗	張喬凱、賴珈均 李政庭、張恩旗 鍾震桂	59
10:45~11:00	D10_07	以分子動力學研究奈米碳管不同挫曲模態的變形型態與機制	張怡玲、范譽馨 胡智捷	60
11:00~11:15	D10_08	★ CMOS MEMS Z 軸微加速度計與電容感測電路之整合及實現	林佳暐、康育齊 陳榮順、林建宏	61
11:15~11:30	D10_09	超聲波震動輔助式雷射微細加工	邱繼正、李永春	62
11:30~11:45	D10_11	新型 MEMS 中心支撐電容式麥克風特性分析	楊政達、黃立嘉 許仁碩	63
11:45~12:00	D10_12	阻抗量測電路系統之設計與應用	許彧祥、蘇育全	64

Oral Session 2　9 月 2 日　16：00～17：30

A2 微系統技術 Nano Material Fabrication and Applications				
主持人: 戴慶良　楊台發			地點: Room 1109	
Time	**Paper ID**	**Title**	**Authors**	**Page**
16:00~16:15	A03_07	聚苯胺摻雜多壁奈米碳管整合電路之葡萄糖感測器	林威邑、戴慶良	66
16:15~16:30	A03_08	★ 以光輔助沉積法沉積鉑奈米顆粒於二氧化鈦奈米顆粒上應用於直接甲醇燃料電池	林峻霆、黃鴻基 楊智仲、蘇育政 朱念南、蕭銘華	67
16:30~16:45	A03_10	Alignment of Liquid Crystal with Nanoporous Anodic Aluminum Oxide (np-AAO) Layer for LCD Application	C- H, T-T Tang, C-Y Hung, R-P Pan,W-L Fang	68
16:45~17:00	A03_11	$Ge_2Sb_2Te_5$ 相變化材料熱傳導係數量測之研究	孫偉哲、黃郁仁 黃胤誠、簡恆傑 謝宗雍、饒達仁	69
17:00~17:15	A03_12	氧化鋅奈米薄膜非揮發性記憶體元件之製程及特性分析	陳昭宇、楊台發 徐冠婷	70
17:15~17:30	A03_20	Formation and characteristics of reactive sputtering deposited ZnNO thin film from n-type to p-type conductivity by thermal annealing	Y-J Chen, T-F Young, C-H Li	71

B2 生醫微流體 Fluidic Micro-components and Systems				
主持人: 傅龍明　施文彬			地點: Room 1108	
Time	**Paper ID**	**Title**	**Authors**	**Page**
16:00~16:15	B04_25	底切蝕刻技術製作微孔洞於超微液滴生成之研究及其製藥應用	藍俊弘、林哲信	72
16:15~16:30	B04_02	★ Rapid Prototyping of PMMA Microfluidic Chips Utilizing a CO_2 Laser	W-J Ju, M-C Wu, R-J Yang, L-M Fu	73
16:30~16:45	B04_08	Hydrodynamic Well for Non-invasive Single Cell Trapping	C-M Lin, C-C Tseng, and Andrew Wo	74
16:45~17:00	B04_10	Experimental and Numerical Investigation into Micro-flow Cytometer with 3-D Hydrodynamic Focusing Effect and Micro-Weir Structure	H-H Hou, C-H Tsai, L-M Fu R-J Yang	75
17:00~17:15	B04_13	A Microfluidics-based Home Use Sperm Quality Chip	Y-A Chen, J-D Huang, C-M. Lin, C-Y Chen, A-M Wo, Vincent	76
17:15~17:30	B04_26	整合層流擾動現象與光纖懸臂樑於微流體晶片之應用	朱伯堯、林哲信 林世偉	77

C2 微致動與傳感器 Micro-optical Devices and Systems				
主持人: 范士岡 李佳翰			地點: Room 1111	
Time	**Paper ID**	**Title**	**Authors**	**Page**
16:00~16:15	C08_26	Focusing Properties of Near-field Plasmonic Fresnel Zone Plates	Y-J Tsai, I-F Yu, Y-W Cheng, J-H Li, S-H Chen, W-H Sheu	78
16:15~16:30	C08_29	利用噴流式旋轉塗佈系統製作 PDMS 軟性模仁	莊承鑫、吳幸昇 蔡嵩玟、莊峰富	79
16:30~16:45	C08_30	應用 DVD 讀取頭技術量測多層膜曲面光學元件	林君維、吳嘉哲 陳志敏	80
16:45~17:00	C08_31	Objective-type dark-field illumination for multi-wavelength fluorescent detection of capillary electrophoresis	S-W Lin, J-H Hsu, C-H Chang, and C-H Lin	81
17:00~17:15	C08_35	步階旋轉式黃光微影製作無接縫滾筒模仁及應用於微透鏡光學膜陣列	李永春、蕭飛賓 陳泓瑋	82
17:15~17:30	C08_44	★ 介電泳致動之液態-液態光波導性質量測	盧羿爻、邱誠樸 范士岡	83

D2 微系統設計、製造封裝與材料技術 Design, Simulation and Testing				
主持人: 林明澤 朱俊勳			地點: Room 1110	
Time	**Paper ID**	**Title**	**Authors**	**Page**
16:00~16:15	D10_13	以光學方法量測微槳型懸臂樑上金屬薄膜材料靜態與動態行為	鄭雅琪、童麒嘉 陳冠綸、曾偉庭 林明澤	84
16:15~16:30	D10_15	電漿輔助化學氣相沉積氮化矽薄膜之破壞與疲勞性質檢測及其在微系統結構可靠度之分析與應用	黃致凱、吳秉欣 歐廣順、陳國聲	85
16:30~16:45	D10_16	不同 Ti 薄膜厚度沉積在周邊 Gaten+p+ contact 的電阻值特性研究和在 70 奈米 512Mb 動態隨機記憶體的 tRCD 問題改善	黃國興、林成利 賴岱鈺、蔡明憲 李再立	86
16:45~17:00	D10_17	具指向性之陣列式壓電揚聲器研究	莊承鑫、黃舜暉	87
17:00~17:15	D10_18	原子層沉積技術之氧化鋅薄膜應力分析	蕭俊卿、黃聖文	88
17:15~17:30	D10_21	★ 應用於直接甲醇燃料電池之奈米等級陽極 CO_2 氣泡行為模式觀測技術	廖振傑、彭顯智 葉宗洸、潘 欽 曾繁根	89

Oral Session 3　9 月 3 日　09：30～11：00

A3 微系統技術 Simulations for Nano Systems & Nano Material Fabrication and Applications				
主持人: 楊啟榮　許光城			地點: Room 1109	
Time	**Paper ID**	**Title**	**Authors**	**Page**
9:30~9:45	A01_05	★ Single dsDNA Manipulation By Controlling DEP Nano Virtual Pore	C-J Chang , P-C Wang , F-G Tseng	91
9:45~10:00	A02_01	由內能變化探討奈米壓痕基材效應之有限元素分析	江智揚、陳國聲	92
10:00~10:15	A02_03	運用平行處理於全原子模型之碳氫化合長鏈高分子(PMMA)奈米壓印成型分析	許光城、周墩桊	93
10:15~10:30	A02_04	Experimental matching method for the two-dimensional numerical simulation of micro-floating zone in laser heated pedestal	P-Y Chen, C-L Chang, S-L Huang, C-W Lan	94
10:30~10:45	A01_02	高深寬比矽基奈米孔洞陣列元件製備	何京諭、王國禎	95
10:45~11:00	A03_18	以濕式蝕刻製作奈米壓印之矽基模板	許哲維、張元震 李永春	96

B3 能源科技　Microdevices for Power Supply and Energy Harvesting				
主持人: 潘正堂　邱一			地點: Room 1108	
Time	**Paper ID**	**Title**	**Authors**	**Page**
9:30~9:45	B06_03	可增加寬頻之振動電磁式發電微系統	呂文隆、黃永茂	97
9:45~10:00	B06_05	以奈米碳管與聚苯胺之複合材作為微生物燃料電池陽極板的研究	林華偉、王金燦 陳博彥、胡毓忠	98
10:00~10:15	B06_06	Modeling and Analysis of a DC Electrostatic Vibration-to-Electricity Micro Power Generator	C-F. Chang and Y Chiu	99
10:15~10:30	B06_08	應用於微型燃料電池之高效能矽基膜電極組開發	彭顯智、葉宗洸 曾繁根	100
10:30~10:45	B06_12	Design and fabrication of flexible piezoelectric ZnO micro-generator with storage systems	C-T. Pan, Z-H Liu, J-S Tsa1, Y-C Chen, J-H Kuang, W-T Chang and Y-C Huang	101
10:45~11:00	B04_04	★ Microflow Cytometer for Three-dimensional Focusing with Sequence Micro-weir Structures	H-C Lee, C-H Lin	102

C3 微致動與傳感器 Mechanical, Thermal, Magnetic Sensors and Actuators				
主持人: 張凌昇 莊承鑫			地點: Room 1111	
Time	**Paper ID**	**Title**	**Authors**	**Page**
9:30~9:45	C07_03	創新次微米多孔性之碳黑 PI 感測晶片於揮發性有機氣體之偵測	古翊航、林哲信	103
9:45~10:00	C07_18	新型 CMOS-MEMS 立體式微磁通閘設計與特性量測	黃文聖、呂志誠 鄭振宗	104
10:00~10:15	C07_19	★ DESIGN AND IMPLEMENTATION OF A NOVEL CAPACITIVE-SENSING MICROPHONE	C-K Chan, W-C Lai, M-C Wu, W-L Fang	105
10:15~10:30	C07_20	出平面 CMOS-MEMS 微型共振器設計分析與實現	劉育嘉、蔡明翰 陳文健、李昇憲 方維倫	106
10:30~10:45	C07_21	A CMOS-MEMS Accelerometer with Tri-axis Sensing Electrodes Arrays	M-H Tsai, Y-C Liu, C-M Sun, W-L Fang	107
10:45~11:00	C08_37	Fabrication and Design of Various Dimensions of Multi-Steps Ashperical Microlens Arrays for OLED Package	C-T Pan, Y-C Chen, M-F Chen, J- P Yur, Y-C Hsu	108

D3 微系統設計、製造封裝與材料技術 Design, Simulation and Testing & Fabrication and Packaging Technologies & Miscellaneous				
主持人: 楊龍杰 王國禎			地點: Room 1110	
Time	**Paper ID**	**Title**	**Authors**	**Page**
9:30~9:45	D10_22	★ 常壓電漿游離質譜系統之開發及其於快速防恐偵測之應用	潘致戎、謝建台 許維仁、楊超榮 林哲信	109
9:45~10:00	D10_24	Design and Simulation of Micro Stent for Renal Artery Disease	H-M Hsiao	110
10:00~10:15	D11_01	可圖案化明膠中碎形微結構之成長	李佳展、馮龍田 高阿福、楊龍杰	111
10:15~10:30	D11_02	陽極氧化鋁膜奈米二極體	張政嶢、王國禎	112
10:30~10:45	D11_03	噴印高分子於微結構裡之固化輪廓成形性探討	杜昆澤、陳錦泰	113
10:45~11:00	D12_01	壓印技術提升發光二極體出光效率之研究	倪慶懷、陳智有 李有璋、黃禹傑 蔡炯祺、蔡宗良	114

Oral Session 4　9 月 3 日　13：30～15：00

A4 微系統技術	Nano Material Fabrication and Applications			
主持人: 李泉 鍾震桂			地點: Room 1109	
Time	**Paper ID**	**Title**	**Authors**	**Page**
13:30~13:45	A03_22	高效能氮氧化物螢光粉(Ca-alpha-SiAlON)之合成	黃姝綺、劉彥群 鍾賢龍	116
13:45~14:00	A03_23	★ 觸媒蝕刻技術應用於矽質奈米柱陣列之研製	黃茂榕、楊啟榮 林峻霆、陳世佳 張峻銘、湯喻翔 蕭銘華	117
14:00~14:15	A03_24	疏水 Polybenzoxazine 應用於介電濕潤元件	楊正臣、王業昇、許耀文、邱誠樸、張豐志、陳俊勳、范士岡	118
14:15~14:30	A03_25	水熱合成法製備氧化鋅之整合型氨氣微感測器	楊閔智、戴慶良	119
14:30~14:45	A03_27	AAO 模板應用於奈米熱電結構之製作	楊啟榮、詹金龍 陳彥翔、傅從順 李明俊	120
14:45~15:00	A03_34	基板偏壓與氮氣流量對氮化鉭薄膜的微結構、電阻率與機械性質的影響	張乃文、鍾震桂	121

B4 生醫微流體	Fluidic Micro-components and Systems			
主持人: 劉承賢 馮國華			地點: Room 1108	
Time	**Paper ID**	**Title**	**Authors**	**Page**
13:30~13:45	B04_15	整合微流體生醫晶片與流式細胞儀分析技術於高效率之人精篩選系統	傅薈廷、黃鴻儒 李金蓉、黃泓淵 饒達仁	122
13:45~14:00	B04_01	A New Microfluidic Chip for Formation of Emulsion Micro-droplets Utilizing a Normally-closed Valve	J-H Wang and G-B Lee	123
14:00~14:15	B04_20	超音波駐波操控具增強生化粒子鍵結偵測效率之晶片研發	馮國華、楊舒翔	124
14:15~14:30	B04_22	以介電加熱法於介電濕潤數位微流體平台實現微液滴加熱	蔣采蓉、范士岡	125
14:30~14:45	B04_14	★A Continuous Microfluidic System for Systematic Evolution of Ligands Exponential Enrichment	Y-H Chen, H-I Lin, S-C Shiesh, G-B Lee	126
14:45~15:00	B04_17	整合聚焦與捕捉功能之可程式化介電泳篩選晶片	莊承鑫、黃耀緯 徐佑銘、吳耀東	127

C4 微致動與傳感器 Micro-optical Devices and Systems & Wireless Communications Devices and Systems				
主持人: 黃義佑 李佳言			地點: Room 1111	
Time	Paper ID	Title	**Authors**	**Page**
13:30~13:45	C08_36	Massive cell/polystyrene beads manipulation with optoelectronic system	H-P Chen,S-M Yang,Y-J Su,Long Hsu,C-H Liu	128
13:45~14:00	C08_39	非對稱微透鏡陣列設計製作研究	楊錫杭、林盈妃 葉茂勳	129
14:00~14:15	C08_40	雙穩態電磁致動式 2x2 光開關之開發	廖信宏、廖柏亭 施順智、蔡東湘 楊燿州	130
14:15~14:30	C08_45	電磁式側向力致動微掃描面鏡	賴騰憲、鄒慶福	131
14:30~14:45	C08_49	應用於光連接網路電熱式驅動光開關元件後製程之研究	蔡健忠、鍾光韋	132
14:45~15:00	C09_50	★具深次微米間隙之高 Q 值整合式 CMOS-MEMS 共振器	陳文健、李銘晃 方維倫、李昇憲	133

D4 微系統設計、製造封裝與材料技術 Fabrication and Packaging Technologies				
主持人: 洪國永 鄒慶福			地點: Room 1110	
Time	**Paper ID**	**Title**	**Authors**	**Page**
13:30~13:45	D11_06	★ A MEMS-based optical pickup unit fabricated and assembled on SOI wafers	C-A. Lin, C- A Chen ,Y Chiu, C-S Wu, H-F Shih	134
13:45~14:00	D11_07	★利用熱能與靜電能於動態流體中以發展高分子聚合物雙凸非球面透鏡新穎之製造技術	洪國永、陳宜課 范朝智、曾繁根 施錫富、邱 一 邱俊誠、方維倫	135
14:00~14:15	D11_08	矽晶太陽能電池抗反射層之微奈米結構陣列製作	楊啟榮、莊宗奇 高瑋鴻、古鎮南 段憶祖、蕭博元	136
14:15~14:30	D11_10	具有微透鏡陣列之晶圓級 LED 構裝	張君銘、陳志明 賴騰憲、黃正翰 鄒慶福、黃榮興	137
14:30~14:45	D11_11	電子紙顯示器之可固化薄膜材料封裝技術	黃莉玲、楊正臣 邱誠樸、范士岡	138
14:45~15:00	D11_12	Magnetic Lifting and Welding to Simultaneously Assembly and Package a Quality-Factor-Controllable Micromachined Inductor	Y-C. Huang, B-H. Jang and W Fang	139

二、壁報論文 9 月 2-3 日

壁報位置	論文編號	論文名稱	作者	頁碼
P1	A01_01	以飛秒雷射製程在透明導電膜材料之探討	鄭仁維、張天立 李有璋、郭詠欣 蔡定凱、陳肇祈	141
P2	A01_04	CF_4 電漿處理對氧化鋁鉿閘極介電層之電性與可靠度研究	C-Li Lin, J-J Honga, S-C Wu	142
P3	A01_06	以調變脈衝式超快雷射在光學微結構之研究	郭詠欣、張天立 蔡定凱	143
P4	A01_07	薄膜晶圓表面奈米粒子散射光之三維偏振分析	劉承揚	144
P5	A03_05	改變磁性奈米粒子種類與靜磁場對磁轉染效率之影響研究	呂怡慶、呂志誠 蘇正煌	145
P6	A03_09	奈米碳管摻雜於碳化矽中並應用於高功率發光二極體固晶散熱研究	洪家偉、甘廣宙 林俊良、張志祥 黃桓俞	146
P7	A03_13	奈米薄膜 Ta-N 的微結構、機械性質與電性探討	張乃文、鍾震桂	147
P8	A03_14	運用玻尿酸以種晶促進成長法製備多形態奈米金與其機制之探討	周志調、張可欣	148
P9	A03_15	感應耦合電漿蝕刻製備次微米氧化鋁圓洞陣列	張峻銘、黃書瑋、黃茂榕、蕭銘華、朱念南、薛文證、馬廣仁、蔣東堯	149
P10	A03_16	奈米結構化藍寶石晶片之光學特性研究	林佑昇、張恩豪、徐文慶、黃國政、葉哲良	150
P11	A03_17	Film Thickness and Chemical Bonding Analysis of Ultra-Thin Film HfO_2 Using Grazing X-ray Reflectometry and X-ray Photoelectron Spectroscopy	Y-Q Chang,W-E Fu	151
P12	A03_19	利用奈米結構氮化銦緻密層製作染料敏化太陽能電池之應用	陳隆建、郭書榮	152
P13	A03_21	原生氧化層效應對鋁金屬誘發非晶矽的電性與孔洞影響	彭政展　、林仁輝	153
P14	A03_26	用沾筆式奈米微影技術製作乳膠球陣列	葉嘉仁、呂慧歆 林啟萬	154
P15	A03_28	Effect of SiO_2 additive on crystalline structure and H_2S sensing performance of CuO-Au-SnO_2 thin film prepared by liquid phase deposition	J-C Chiou, S-W. Tsai, L-J Shieh, K-C Hou, C-W Chang, Y-C Lin, Y-C Huang	155

P34	B05_03	Glass Microprobe with Multi-electrode Styles Implemented by Silicon Via Structure	Y-T Lee, C-W Lin, Y-C Chang, W-L Fang	174
P35	B05_04	溫感性高分子應用於具釋放細胞功能之細胞篩選晶片	汪俐穎、陳玉暄 曾繁根	175
P36	B05_05	微機電技術發展靜電式相位元件以獲得電子顯微鏡生物增強對比影像	林立婷、黃祖緯 陳福榮、曾繁根	176
P37	B05_06	以共平面式介電濕潤晶片操控懸浮之包覆式液珠形成人工脂質雙層膜	林依縈、范士岡	177
P38	B05_07	DNA Aptamer-integrated Extended-gate Field-effect Transistor Biosensor for Tumor Marker Recognition	M-Y Lin, Y-P Lai, N-N Chu, Y-S Yang, H Chen	178
P39	B05_09	Atmospheric Micro-Plasma Chip for High-speed Mass Spectrum Analysis Fabricated Utilizing A Novel Bonding-free Fabrication Process	S-M Kuo, C-J Pan, J-T Hsieh, C-H Lin	179
P40	B05_13	磷光相位量測技術於溶氧濃度微感測器檢測之研究	黃士豪、曾偉純	180
P41	B05_15	微陣列電極晶片進行電穿孔基因轉殖之研究	鍾永強、廖偉傑 黃毓慈	181
P42	B06_01	Micro-Energy Harvester Based on Piezoelectric Nanorods	W-Y Chang, T-H Fang, H-J Lin, C-H Chu	182
P43	B06_02	微型直接甲醇燃料電池之奈米碳管承載白金觸媒電極耐久性測試	吳宜萱、郭妍妏 吳仁貴、葉宗洸 蔡春鴻、曾繁根	183
P44	B06_04	Micro Power Generator by using CMOS MEMS	L-C Chou, Y-L Lai, S-C Huang, J-C Chiou	184
P45	B06_09	微型直接甲醇燃料電池陽極端微噴霧式進料系統製作	葉易橏、彭顯智 林葆喜、凌守弘 蔡麗端、曾繁根	185
P46	B06_10	Design and Optimization of an AC Electrostatic Vibration-to-Electricity Micro Power Generator	H-C Liu, Y Chiu	186
P47	B06_11	CMOS-MEMS 高效率微熱電發電機之設計與製作	蔡文榮、戴慶良	187
P48	B06_13	奈米碳管做為觸媒載體之低溫高效能微型甲醇重組反應器研製	賴淑萍、王奕勛、黃國洋、黃鈺軫、曾繁根	188
P49	B06_14	利用半開放迴流系統溫度調控合成高效能奈米觸媒應用於 μDMFC	吳宜萱、龔欣玫 王鈞顯、葉宗洸 蔡春鴻、曾繁根	189
P50	C07_01	熱處理對二氧化錫氣體感測層之氧氣感測器感測性能影響之研究	王盟翔、王譽程、王禹翔、李佳言、傅龍明	190

國立中山大學
三十而立·砥柱中流

專題演講

Keynote Speech 1

1. Dr. Kazuo Sato (現任職 Japan, Nagoya University)

個人介紹:

Dr. Kazuo Sato 於1982 年於日本東京都大學取得博士學位，在攻 讀其間開始兼任日立有限公司感測器研究團隊之研究專員，擁有豐富產業發展經驗，至1994年在Nagoya大學擔任微系統工程研究所教授，2006 年時擔任Tokyo Institute of Technology 精密與 慧研究所之客座教授。其曾經獲得 Japan Society for Technology of Plasticity(1986)、日本精密工程科技獎(1989)、JSME 企業創造獎(1999)、IEEJ 傑出論文獎等(2008)。其傑出表現於1997~2007 年分別在IEEE MEMS 擔任會議主席，並且亦是Microsystem Technology、Micromechanics and Micro engineering 與Precision Engineering and Manufacturing 期刊之編輯委員，其研究成果有200 篇以上發表於國際各期刊中。

MEMS need science: Challenging the mysteries of anisotropic etching of Si

Kazuo SATO

Micromachining & MEMS Laboratory, Nagoya University, Japan

Abstract

Micromachining & MEMS Laboratory, Nagoya University is pursuing research in two directions. One is creating new device-concepts and those prototyping, and the other is materials science focusing on physical and chemical properties of Si as a MEMS material. As a part of the latter research, we are investigating physics of anisotropic etching of single crystal silicon and also quarts to meet demands of MEMS industries, which are still facing difficulties due to mysteries in fabrication processes. We firstly characterized the anisotropy in etch rate for a number of orientations and made it possible to analyze etch profiles for arbitrary masking patterns. Secondary, we investigated the mechanisms of anisotropy change according to a difference in etching conditions. Effects of a small amount of impurities and additives in alkaline etching solutions on the etch rates of Si were investigated. Mechanisms of a drastic change in anisotropy by the addition of surfactant to etching solutions are clarified. Such basic research allowed us to develop new processes extending a variation of 3-D structures fabricated by wet etching process.

1. Etch rate characterization and etching simulation

We established the method for characterizing etch-rate anisotropy as functions of crystal orientations. We commercialized an etch-rate database ODETTE, and etching simulation system Fabmeister-ES (former name: MICROCAD) by applying our characterization methods.

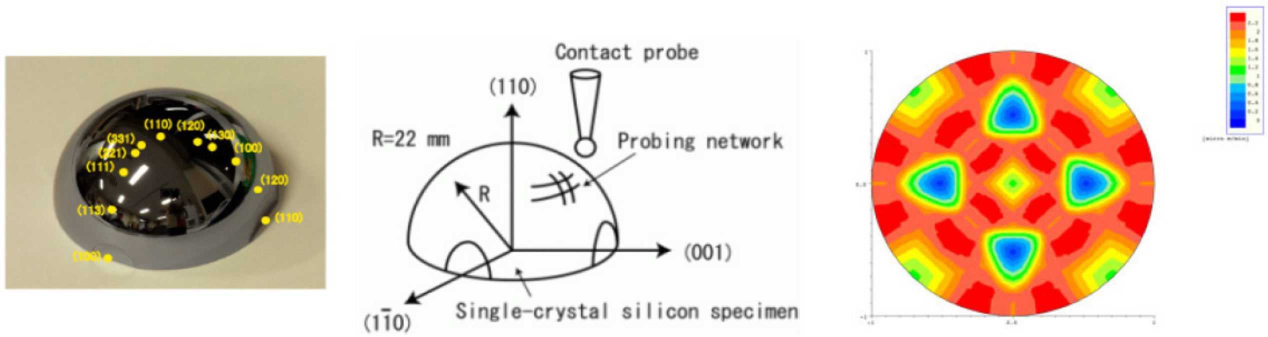

Fig. 1 Characterization of etch rate anisotropy for total orientations. Hemispherical Si specimen (left) is etched in different etching conditions. Measuring the profiles before and after etching provides us etch rate for any orientations (middle). An example of etch rate contour map for 40%KOH solution (right).

2. Etching physics and its application to MEMS structuring

We are investigating etching physics for explaining a change in anisotropy. A multidisciplinary approach is necessary by combining scientists of different fields such as physics and chemistry. Our collaboration partners in academia are Twente Univ. in etching models, Helsinki Univ. Tech. in the first-principle calculation, and Tohoku Univ. in solid-liquid interface analysis. As the results of our collaboration research, it turned out that some of the conventional common knowledge in etching must be rewritten as follows.

(1) Etch rate ratio among orientations must not be explained by the number of dangling bonds of an atom on an ideally flat crystal surface. **Atomic steps** schematically shown in Fig. 2 existing on a crystal surface which are easily attacked by solutions are dominating etch rates of silicon.

(2) Effects of cations so far neglected in etching reaction became evident. Using the first-principle calculation, it was proved that a small amount of Cu-ion can pin up the movement of Si atomic steps resulting in a decrease in etch rate and also micro pyramids formation.

(3) When a small amount of **surfactant** Triton X-100 is added to TMAH solution, the etch rate drastically changed as shown in Fig. 3. The reason why the etch rate for (110) decreases under the existence of the surfactant was recently clarified by means of in-situ FTIR solid-liquid interface analysis. It is due to the selective adsorption of the surfactant molecule to the crystal orientations such as (110) and (111), while little to (100) as shown in Fig.4.

(4) Anisotropic wet etching on Si (100) was so far believed resulting in a rectangular etched recess defined by (111). However, recess of **any round profiles** (Fig. 5) can be etched on (100) using TMAH with a surfactant. This means we can fabricate a new type of the 3-D shapes etched by wet processes.

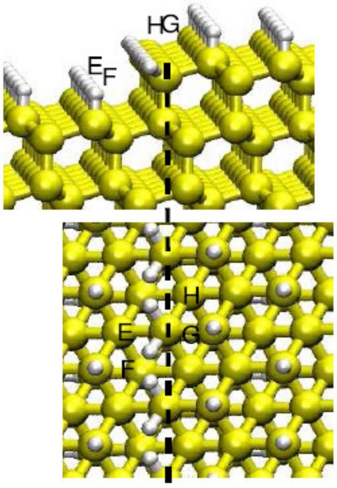

Fig.2 Atomic steps on Si(111) .

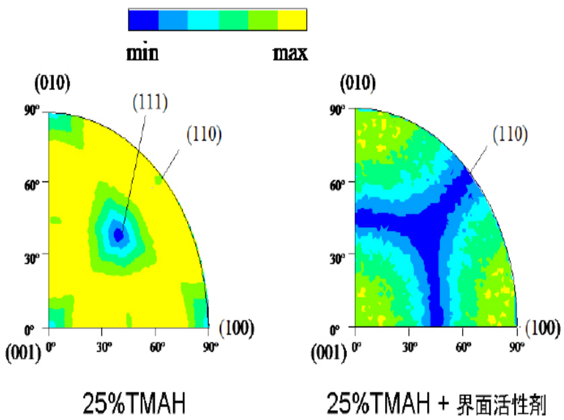

Fig.3 Effects of a surfactant in TMAH solution on a change in anisotropy of etch rate.

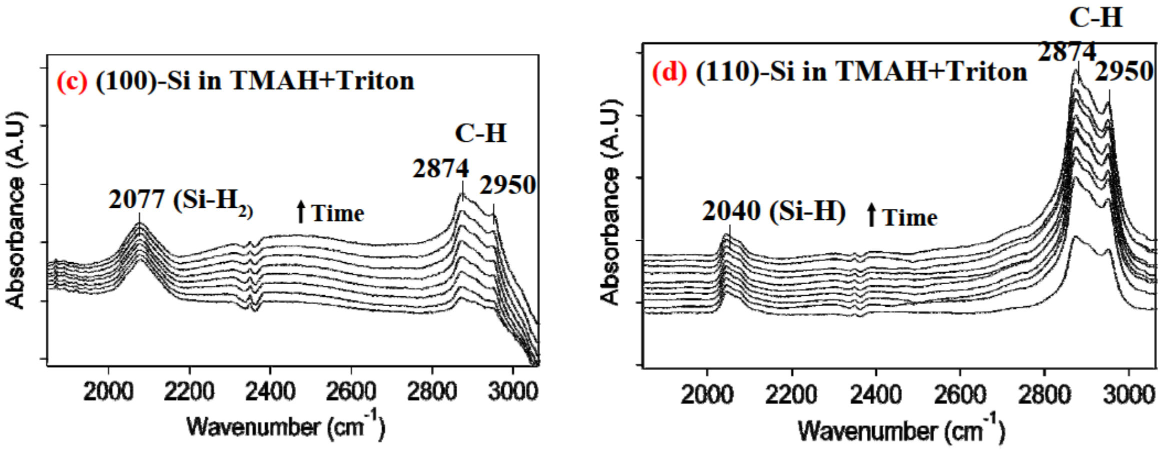

Fig.4
Selective adsorption of surfactant molecule on to the Si(110) observed by in-situ FTIR spectra, resulting in a depression of etch rate for that orientation.

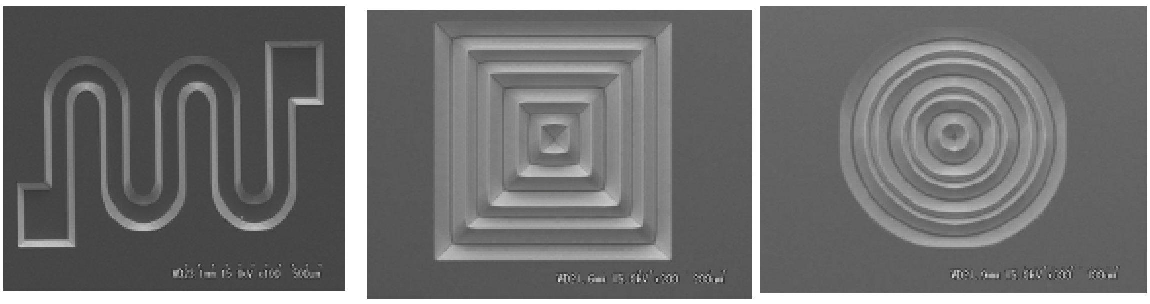

Fig.5 Conformal etch profiles on Si(100) using 25%TMAH solution with 0.1% Triton.

Keynote Speech 2

2. Dong-Qing Li（現任職於Canada, Waterloo University)

個人介紹:

Dr. Dong-Qing Li 於1991年在多倫多大學得到博士學位。爾後開始於1993年，任教於Alberta 大學之機械工程學系，1999 年時正式升為正教授。同年亦獲得McCalla 研究學者獎，2000 年後回到母校多倫多大學的機械工程學系擔任該系所專任教授。而 2005 年10 月至2008 年8 月於Vanderbilt 大學擔任講座教授。2008 年9 月，亦兼任Waterloo 大學微奈米流體學門的講座教授。Dong-Qing Li目前致力於生物晶片與微奈米相關領域技術之研究，其研究成果約有210篇發表於國際期刊並有10餘本著作，目前亦是國際高 Impact Fact期刊Microfluidic and Nanofluidic之主編輯。

Applications of Electrokinetic Microfluidics in Lab-on-a-Chip Devices

Dongqing Li

Department of Mechanical and Mechatronics Engineering

University of Waterloo

Abstract

Imagine holding a business-card-sized, fully functional biomedical diagnostic lab in your hand! A lab-on-a-chip (LOC) is a miniaturized biomedical laboratory built on a thin glass or plastic plate with a network of microchannels, electrodes, sensors and electronic circuits. The lab-on-a-chip devices can duplicate the specialized functions as their room-sized counterparts, such as clinical diagnoses of bacteria, viruses and cancers.

Because of the size of the microchannels, the amount of the liquids involved in such a LOC is on the order of nanoliters, and hence the samples and reagents consumption is significantly less than that required in conventional lab tests. Consequently, the reaction and test time is dramatically reduced. Furthermore, using the microfabrication technology, we can easily make many parallel microchannel systems on a single chip, so that one chip can perform multiple tests at the same time. Electrokinetic microfluidics provides unique advantages to LOC devices. Because of using electrical fields to control all the operations on a chip, the chip has no mechanical moving parts, no external pumps, tubing and valves, etc; multiple steps of a test can be conducted automatically on a single chip. This makes the lab-on-a-chip devices truly portable. The lab-on-a-chip technology is particularly useful for point-of-care and field applications. Clearly, the lab-on-a-chip technology as tools in analytical chemistry and biomedical sciences has enormous potential in developing new technology and reducing the cost.

To realize a specific biomedical or biochemistry assay on a lab-on-a-chip device, the lab-on-a-chip device must be able to perform the following microfluidic functions on a single chip: pumping, flow switching, mixing samples/reagents, sample dispensing and separating molecules and cells. All these microfluidic functions can be realized by the electrokinetic means such as electroosmosis, electrophoresis and dielectrophoresis.

Microscale electrokinetic phenomena originates from the electrostatic charges or

induced charges at the solid-liquid interfaces and liquid-fluid interfaces and the interactions of these charges with the applied electric field. Essentially all

solid and liquid surfaces in contact with aqueous solutions have electrostatic charge. These charges attract the counterions and repel the coions in the solution and form the electric double layer (EDL) near the solid-liquid or liquid-fluid interface. The interaction of the net charge in the EDL with the applied electric field moves these ions and, via the viscous effect, generates the liquid motion. This is the electroosmotic flow. R Relative to the surrounding liquid, the motion of a charged particle driven by an applied electric field is called the electrophoresis. Electroosmotic flow of the liquid and the electrophoresis motion of the charged particles are two key methods used in transport and manipulation of liquids, molecules and cells in microchannels. In addition to electrostatic charge effects, electric field can induce electric charge/polarization on dielectric particles. The interaction of the induced charge/polarization with a non-uniform electric field can also create the particles' motion, called dielectrophoresis. Dielectrophoresis has been used to manipulate motion of particles such as plastic particles and biological cells in microchannels. This presentation will explain the principles of these electrokinetic phenomena and their applications in LOC devices.

In addition, several non-linear electrokinetic phenomena will be introduced, including electrowetting, dielectrophoresis and induced-charge electrokinetics.

In this presentation, the following LOC devices will be discussed.

- Real-time PCR Lab-on-a-chip detection technology: The Real-time PCR is a direct, rapid, quantitative and extremely sensitive technique for detecting a tiny amount of bacteria (e.g, E. coli, anthrax), viruses, and cancers by detecting a fluorescent signal produced proportionally during the amplification of a specific DNA sequence in a sample.

- Immunoassay lab-on-a-chip for detecting bacteria, viruses (e.g., HIV, SARS, anthrax and BSE (mad cow)) and cancers. The detection on this chip is based on antigen-antibody reactions. This chip is a fully automatic handheld immunoassay laboratory, with high accuracy and low cost. It can simultaneously detect multiple pathogen targets from multiple patient samples on a single chip (in 25 minutes)

- DC-Dielectrophoresis (DC-DEP) lab-on-a-chip for separating cells and bacteria by size from biofluids. This method is based on a physical phenomena—DC-dielectrophoresis, can continuously separate, for example, white blood cells or bacteria from blood, without cell labeling. The device has no mechanical moving parts and no filters.

- Flow cytometer Lab-on-a-chip: This fully automatic handheld flow cytometer chip device can separate, count and detect various blood cells (e.g., CD+4) from a drop of blood.

- Cellular lab-on-a-chip for single cell analysis. Such a lab-on-a-chip can separate a single cell from a population of cells, put the cell in a micro-chamber in the chip and then deliver reagents to the selected cell. A key capability of this chip is to control the micro-environment of the cell chamber in terms of the temperature, the nutrient and drug concentration gradients around the cell. Such a cell lab chip allows controlled, quantitative studies of living cells and has enormous potential in drug discovery and other pharmaceutical research and development. On-chip cancer tumor cell culture and cancer cell immunoassay have been successfully demonstrated.

Future development of LOC technology requires developing advanced photonics and optic technology for (1) on-chip manipulation of single molecules; (2) integrated and sensitive on-chip detection of biochemical reactions; (3) nanoscale fluidic visualization.

Keynote Speech 3

3. Ruey-Shing, Huang (現任職於香港SAE Magnetics (HK) Ltd.)

個人介紹:

黃瑞星博士先後於1969 年至1978 年於國立交通大學取得碩士學位及於澳洲New South Wales 大學取得博士學位，之後1978 年於紐約Cornell(康乃爾)大學電子工 程系所擔任博士級研究員，並致 力於 MESFET/SOS 應用相關之研究。1979~1986 年回到台灣清華大學電子工程研究所擔任專任教授，其目前致力於 MOS 積體電 路製程技術及一些Solid-Sensor 之研究，其間於1983~1984 年他至New Mexico, Albuquerque 習得有關MNOS 技術並接著於1986~1994 時至New South Wales 研 究Solid-Sensor 等相關技術。自1994 年起其再度回到清華大學電子工程研究所致力於微機電研究中，亦曾服務於國科會微機電研究中心，個人之研究著作亦有刊登於國際期刊中。現擔任SAE Magnetics (HK) Ltd. 顧問。

A Large Area Large Angle Si Scanning Micro Mirror

Star Huang

SAE Consultant

Emeritus Professor

National Tsing Hua University

Abstract

Silicon scanning micro mirror has been around for some years and billions of micro mirrors has been used in consumer products such as DLP in desk top projectors and hand held pico projectors. However, these micro mirrors are either small area or small scanning angle micro mirror devices. The application of scanning micro mirror in laser printer requires large area and large angle micro scanning mirror; large area for better resolution and large angle for page wide scan at short working distance. This talk will present the concept to design a large area large angle scanning micro mirror by using cascade distributed hinges to achieve these goals, the key fabrication technologies, including the backend testing package and testing. The specifications of scanning mirror for high speed high resolution laser printers are outlined and the detail performance measured results of the fabricated devices will be presented including some preliminary reliability test data.

Keynote Speech 4

4. Ji-Jun Zhao（現任職於大連理工大學）

個人介紹：

趙紀軍博士於1996 年於南京大學物理系獲取博士學位後，接著1997~2001 年先後服務於義大利國際理論物理中心(TCTP) 及美國北卡大學物理系擔任博士後研究員，並在 2001~2002 年於美國北卡大學擔任助理教授，2003~2005 年至美國華盛頓州立大學衝擊波物理研究所擔任研究員，2006 年起，其回國擔任大連理工大學物理與光電工程學院之教授並兼任高科技研究院副院長，2007 年起轉於擔任計算材料研究所所長。趙紀軍博士主要研究領域為計算凝聚態物理和計算奈米科學，其研究多次獲得教育部、國家自然科學基金會等數個計劃型補助，更擔任國際期刊Journal of Atomic and Molecular Sciences(JAMS)的執行主編、SCI 國際期刊Journal of Computational and Theoretical Nanoscience編委及核心期刊《原子與分子物理學報》編委，並任職於中國金屬學會材料科學分會材料計算與模擬學術委員會常委理事、中科院上海技術物理所客座研究員、中國地震局地震預測研究所客座研究員。其研究成果亦多次發表於各論文、期刊中，並應邀為國際SCI 和國際學術專著撰寫綜述10 餘篇，經SCI 檢索，至今累計他引用超過1800次，最高單篇引用300 餘次。

First-principles simulations of carbon nanostructures

Jijun Zhao

Key Laboratory of Materials Modification by Laser, Ion and Electron Beams (Dalian University of Technology), Ministry of Education, Dalian 116024, China.

College of Advanced Science and Technology and School of Physics and Optoelectronic Technology, Dalian University of Technology, Dalian 116024, China.

Abstract

In the past two decades, there have been tremendous interests in the carbon nanostructures of different dimensions, including fullerene, nanotube, graphene, and nanodiamond, etc. Using first-principles method incorporated with some empirical/semiempirical approaches, we have recently investigated the structural, mechanical, electronic, and transport properties of a variety of carbon nanostructures [1-5]. In this presentation, I will briefly illustrate some of these progresses from our group, with emphasis on the fascinating physical properties of these carbon nanostructures associated with potential applications.

References

[1] L. Wang, K. Lee, Y. Y. Sun, M. Lucking, Z. F. Chen, J. J. Zhao, S. B. Zhang, ACS Nano **3**, 2995 (2009).

[2] X. Jiang, J. J. Zhao, C. Q. Zhuang, B. Wen, X. Jiang, Diam. Rel. Mater. **19**, 21 (2010).

[3] L. Z. Liu, H. L. Gao, J. J. Zhao, J. P. Lu, Nanoscale Res. Lett. **5**, 478 (2010).

[4] S. J. Guo, X. L. Pan, H. L. Gao, Z. Q. Yang, J. J. Zhao, X. H. Bao, Chem. Eur. J. **16**, 5379 (2011).

[5] H. L. Gao and J. J. Zhao, J. Chem. Phys. **132**, 234704 (2010).

Academia-Industry Consortium For Southern Taiwan Science Park

中華民國南部科學園區產學協會

協會業務內容：

1. 結合南部大專院校及南科園區資源，致力於提供人才培訓、人才與技術媒合、及會議展覽活動辦理之服務。
2. 協助南部大專院校及南科各單位辦理國內及國際研討會及大型活動，提供專業服務，以提昇會議品質及國際形象。
3. 協助南部大專院校及南科產業辦理徵展作業及展覽規劃。
4. 協助產業界爭取政府專案計畫資源於研發技術及人才訓練。
5. 協助協會會員於相關活動辦理之宣傳與公關作業。

歡迎您的加入！！！！

聯絡電話：06-2757575 ext.32115

06-2384278/ 06-2096455

協會：台南市東區大學路一號

（自強校區工學院系統系八樓）

協會網址：https://www.aicsp.org.tw

聯絡人：黃詩芸小姐、侯翠玲經理

中華民國微系統暨奈米科技協會
Nanotechnology and Micro System Association, Taiwan

協會簡介

『中華民國微系統暨奈米科技協會』成立於1995年2月。秉持著協會的宗旨提供更多元化的服務，以期會員透過協會活動交流獲得提升技術及產值之綜效。

年度活動

1.透過協會專業網站（http://www.nma.org.tw/），分享國內外研討會與會報告資料/市場資訊，提供會員最新訊息。
2.發佈newsletter分享新訊息（兩星期一次）。
3.發行半年期會刊使會員了解國內外專業知識以及文章。
4.舉辦奈米工程及微系統技術研討會暨微系統暨奈米科技應用展。
5.舉辦年度優良產品獎、服務貢獻獎、微奈米科技獎章、微系統與奈米科技產業貢獻獎。
6.舉辦技術研討會/成果發表會/會員大會。

會費

單位:新台幣/元

會員種類	入會費	常年會費（一年期）	永久會員
個人會員	100	500/年	6,000
團體會員	1,000	2,000/年	24,000
學生會員（需繳交學生證影本）	50	50/年	無表決、選舉等權利

入會辦法

請填妥適用表格（協會網站提供http://www.nma.org.tw/），
連同劃撥收據，傳真或郵寄給楊珮民小姐。
電話：(06)384-7152 傳真：(06)384-7294 E-mail：min@itri.org.tw

即日起加入協會即贈送書籍

書籍名稱：台灣奈米科技-從2004到嚮往的大未來、圖解奈米科技、圖解奈米應用技術（每本原價：NT$600元）

永久會員/團體會員：**贈送3本**

一般會員/學生會員（加100元）：**贈送1本**(3本擇1本)

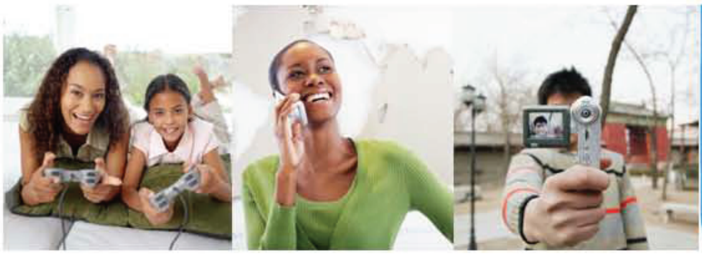

工業技術研究院
Industrial Technology Research Institute

南分院微系統科技中心

以微感測、微致動及系統微小化構裝技術，發展健康、安全、娛樂等隨身數位化智慧微系統，使每個人都能獲得 *無微不至* 與 *無所不在* 的優質生活照顧。

微系統核心技術與應用

CMOS MEMS 技術

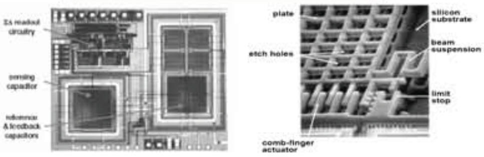

MEMS 封測技術

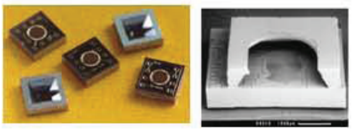

MEMS 設計技術

- 壓力感測元件
- 慣性感測元件
- 光學元件
- 射頻元件

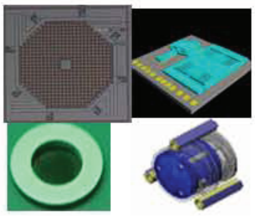

微系統應用技術

- 智慧感知模組
- 微型致動模組
- 系統微縮構裝

產業應用

行動通訊

醫療保健

消費性電子

資訊電子

車用電子

微系統技術研發與服務

▸研發方向

- ◎ 智慧互動(動作感知元件與應用)
- ◎ 電聲感測(MEMS麥克風)
- ◎ 微霧化器(醫療級)
- ◎ 隨身照護(無線生理監控貼片)
- ◎ 微型致動(防震變焦模組)
- ◎ 微系統開放實驗室

▸產業聯盟

- ◎ 微機電產業發展聯盟
- ◎ 微電聲產業聯盟 (http://matia.org.tw/)
- ◎ 微機電LAB使用者聯盟 (http://memsclub.itri.org.tw)
- ◎ CMOS MEMS產業策略聯盟
- ◎ 動作感知技術創新應用產業策略聯盟

▸聯絡方式

▸聯絡窗口：黃豈苙 小姐

▸聯絡電話：06-3847128

▸傳真電話：06-3847294

▸電子信箱：huang0606@itri.org.tw

▸聯絡地址：70955 台南市安南區工業二路31號研究一館206室。

～ 歡迎洽詢 ～

BUEHLER®

Quality At Work!

ISOMET 4000 / 5000 微電腦控制型線性精密切割機

- 全自動線性精密切割機
- SmartCut 智慧切割功能
- 樣品定位精度為 1-2 μm ， LCD 顯示
- 950W 功率馬達，轉速可達 5000rpm
- 切割片直徑 3"-8"（75-200mm）
- 程式記憶：標準切割方式 35 組，自定程式 20 組
- 自動連續切片：1-100 片

EcoMet Pro 系列研磨 / 拋光機和 AutoMet 系列自動研磨頭

- 工作區 LED 照明
- 全機一體成型鋁合金鑄造機身，抗腐蝕、防汙及防剝落表面塗裝
- 單點施力 / 中央施力雙模式
- 可伸縮沖洗水龍頭以及工作盤 360 度冷卻
- 製備結果可重複性高
- 高扭力馬達
- 彩色液晶觸控式螢幕
- 圖文介面以及多種語言顯示（包括中文）
- Z 軸移除量控制
- 內置製備方法資料庫

PSC 專業 熱忱 團隊合作
汎達科技有限公司
PENTAD SCIENTIFIC CORPORATION

總公司：新竹市光復路二段 295 號 6 樓之 2
TEL：03-5728466 FAX：03-5728467
高雄辦事處：高雄市左營區大順一路 91 號 7 樓之 4
TEL：07-5565238 FAX：07-5565637
www.pentad.com.tw pentad@pentad.com.tw